ANALYSES OF CONTAINMENT STRUCTURES WITH CORROSION DAMAGE[1]

Jeffery L. Cherry
Sandia National Laboratories
PO Box 5800
Albuquerque, New Mexico 87185-0744
U.S.A.
(505)-844-0090

ABSTRACT

Corrosion damage to a nuclear power plant containment structure can degrade the pressure capacity of the vessel. For the low-carbon, low-strength steels used in containments, the effect of corrosion on material properties is discussed. Strain-to-failure tests, in uniaxial tension, have been performed on corroded material samples. Results from the tests were used to select strain-based failure criteria for corroded steel. Using the ABAQUS finite element analysis code, the capacity of a typical PWR Ice Condenser containment with corrosion damage has been studied. Multiple analyses were performed with the locations of the corrosion on the containment, and the amount of corrosion varied in each analysis.

INTRODUCTION

Corrosion damage has been found in a number of existing containments (Shah et al., 1994). Tests conducted by Sandia National Laboratories on scaled containment models and analytical efforts have demonstrated that containments without corrosion can resist static internal pressures that are well above the containment's design pressure without significant leakage (Jung, 1984; Koenig, 1986; Reese and Horschel, 1985; Miller, 1990; Fanous et al., 1993). However, corrosion found in containments of operating nuclear power plants has prompted concerns regarding the capacity of the corroded containment to withstand accident loadings.

Corrosion of containments may reduce the margin between the design and failure pressure and thus might increase the probability of containment failure under severe accident loadings. Comparisons of the shell thickness after corrosion with the ASME Code minimum allowable thickness gives some indication of the reduction in containment capacity. However, the nature and the location of the corrosion must be considered to determine how much the affected areas degrade the ultimate capacity of the containment. For example, considerable corrosion in an area with excess thickness may not affect the ultimate capacity, while minor corrosion in a critical area would lower the ultimate capacity.

Three subjects have been examined in this paper. The first topic consisted of understanding corrosion damage and material properties of corroded steel. Next, finite element modeling options and associated "failure" criteria were examined. Finally, multiple analyses were performed for a typical PWR Ice Condenser containment, with the amount of corrosion and the location of corrosion varied in each analysis.

MATERIAL PROPERTIES OF CORRODED STEEL

Damage Mechanisms

Corrosion and other types of degradation are usually categorized according to the mechanisms that cause the damage. For the low-carbon low-strength steels used in containment structures, the categories of corrosion typically listed in textbooks, handbooks, and other reports can be condensed to two major types of damage. These mechanisms (Fig. 1) are:

- *Loss of section*. General (uniform) corrosion, galvanic action, differential aeration, and chemical attack all cause a reduction in the material cross-section. The section becomes thinner as the shell corrodes, and this results in a reduction in strength because of the reduced cross-section. Rough and uneven corrosion surfaces cause strain concentration regions, and failure can occur at lower-than-expected global strains because of tears that initiate in the strain concentration regions.
- *Local pits*. Local pits can be caused by pitting corrosion, crevice corrosion, or microbially influenced corrosion. This type of damage consists of small holes in the metal surface. The amount of metal that is actually corroded away by pitting is usually a very small percentage of the cross-section, so there is no appreciable reduction in strength. Failure can occur at lower-than-expected global strains because of tears that initiate in the

[1] This work was supported by the U.S. Nuclear Regulatory Commission and was performed at Sandia National Laboratories, which is operated for the U.S. Department of Energy under Contract DE-AC04-94AL85000.

DISCLAIMER

strain concentration regions at pit discontinuities. However, local pits can penetrate the steel shell and cause the vessel to leak.

If the density of pits becomes large enough, the pits can grow together and result in a loss of cross-sectional area. These two types of damage often occur simultaneously, so that damage is a combination of both categories.

Corroded material has virtually no strength and uncorroded material retains virgin material properties. A reduction in strength of a corroded structural member is caused by a reduction in cross-sectional area. Also, a reduction in ductility is caused by stress and strain concentration regions at discontinuities such as pits or rough surfaces.

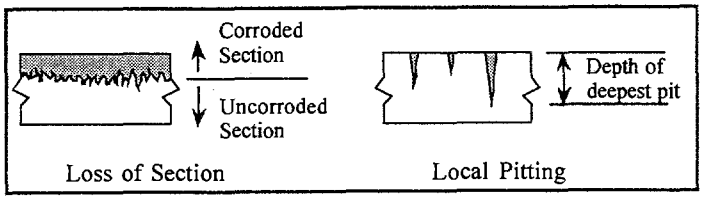

Figure 1. Corrosion damage modes.

Degradation Mechanisms That Do Not Apply

Other types of degradation, such as intergranular and transgranular stress corrosion cracking and hydrogen embrittlement, do not affect the low-carbon low-strength steels used in containment structures. Radiation levels near the containment wall are low enough that radiation embrittlement does not occur.

Corrosion fatigue is not a concern for containment vessels. The ductile carbon steels used in containment structures are not very susceptible to low-cycle fatigue, and the few events which could cause large stresses occur a very limited number of times. Large stresses, but still well below yield, result from pressurizing the vessel to perform leak tests. Several events, such as a large earthquake, could cause a few cycles with elastic or even plastic stresses in the containment structure. Other events that could cause plastic behavior are severe accidents that result in large internal pressure loads. In each of these cases, the number of cycles is small. A fatigue curve in the ASME design code (1992) shows that the ductile steels used in containment structures can be cycled up to yield stress about 5000 times without failure. They can be cycled past the yield stress to 1% strain about 40 times without failure, and they can be cycled to 2% strain about 10 times without causing a failure. These data are for uncorroded steel; Shigley (1983) reports that corrosion reduces the fatigue life by as much as 40%. For containment structures, it is very unlikely that the small number of load cycles will be sufficient to cause fatigue failure or fatigue-related damage.

Welded Properties

When subjected to severe loads, it is common for welded structures to fail in the weld or in the heat-affected zone. However, for the low-carbon low-strength steels used in containment structures, testing has shown that failure occurs away from the weld area. Based on test data (*Structural Alloys Handbook*, 1989), the weld is not the "weak link" in structural failure of A516 or SA212 steels. During uniaxial tension tests, these materials failed in the base metal and not in the weld zone. Of course, a significant crack in the weld zone could cause brittle fracture, just as a large crack in the containment wall could cause brittle fracture. However, corrosion damage found in actual containments has not shown this kind of degradation along weld seams.

CORRODED COUPON TESTS

In order to experimentally measure the structural degradation caused by corrosion, several 0.159 cm thick A516 Grade 70 steel plate samples were corroded in a ~95°C magnesium chloride solution and then tested to failure in uniaxial tension. The plates were placed in a vertical position with about 6.5 cm of each plate submerged in the hot solution; 16 cm was above the waterline with a temperature of ~95°C and humidity levels near 100%. One plate was corroded for a period of 1 week, another for 3 weeks, and the last for 6 weeks. The corrosion products were then removed from the plates by scraping, wire brushing, and using "Naval Jelly" rust remover, so that only the uncorroded steel remained.

Damage to the first plate consisted of general corrosion and pitting. The average thickness decreased by about 5%, but pits and pockmarks were visibly deeper than the material surrounding them. Damage to the second plate was similar, except that the average thickness decreased by about 10%. In the third plate, the pits and pockmarks were deeper and the surface was more irregular (Fig. 2). The average thickness of this plate decreased by about 20%.

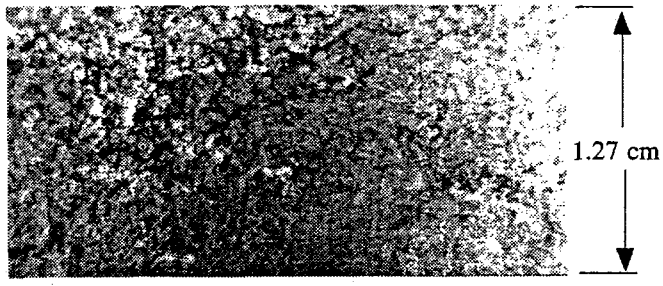

Figure 2. Photograph of coupon with 20% corrosion.

Five standard ASTM dog-bone-shaped tensile coupons were cut from each of the corroded plates, and five coupons were taken from an uncorroded control plate. All twenty coupons had a gage length of 5.08 cm. To ensure uniformity among the coupons, they were all oriented in the same rolling direction, and were all taken from the same plate stock.

On each corroded coupon, thickness measurements were made on a 3 by 17 grid (spaced 0.508 cm apart, in both directions), for a total of 51 measurements per coupon. Initially, the coupons were 0.177 ± 0.0003 cm thick. After corrosion, the coupons with about 5% corrosion were between 0.160 and 0.175 cm thick. The coupons with about 10% corrosion had thicknesses ranging from 0.150 to 0.170 cm and those with about 20% corrosion were between 0.122 and 0.160 cm thick. For each coupon, the average thickness was determined by averaging the 51 thickness measurements. The average cross-sectional area was estimated to be the average thickness multiplied by the width of the specimen.

The coupons were tested to failure in uniaxial tension in accordance with ASTM Standards (1991). Data measured during the

tests consisted of applied force and percent-elongation-in-a-5.08-cm-gage-length. Engineering stress was calculated by dividing the measured force by the average cross-sectional area of the coupon.

Engineering stress versus percent elongation data is shown in Figures 3, 4, and 5. The uncorroded coupons reached about 24% elongation before significant necking began, and about 28% total elongation before failure occurred.

Coupons that were corroded approximately 5% through the thickness reached the same stress levels as the uncorroded specimens, but necking of the specimen began at about 13% strain, and total strains at failure were around 16% (Fig. 3). Three out of the five coupons with this amount of corrosion experienced necking that was outside the 5.08 cm extensometer length. These three coupons show an abrupt drop in load with no further elongation of the specimen. If necking had occurred inside the gage length, then the stress-strain curves would have rolled over gradually, as occurred for the other coupons.

The coupons that were corroded approximately 10% through the thickness reached the same stress levels as the uncorroded specimens, but necking began at about 12% strain (Fig. 4). Four out of the five coupons with this amount of corrosion experienced necking that was outside the 5.08 cm extensometer. Although all five coupons were tested, the test data were accidentally lost on three of the specimens. Therefore, only two curves are available; both specimens necked outside of the gage length.

The coupons that corroded approximately 20% through the thickness reached stress levels that were about 4% less than the stress levels reached by the uncorroded specimens (Fig. 5). This slight decrease in stress is a result of calculating stress using the average cross-sectional area, while the cross-sectional area varied along the length of the specimen; failure occurred in an area that had a lower cross-sectional area than the average. The limited number of thickness measurements, three across the width of the specimen, were not enough to determine what the minimum cross-sectional area really was. However, the thickness measurements nearest the failure locations averaged about 3% less than the overall average that was used to calculate the stresses. Necking of the specimens began at about 14% strains. All of the coupons with this amount of corrosion necked inside the extensometer length.

The approximately 50% reduction in elongation for the corroded coupons was not caused by hydrogen embrittlement effects from the accelerated corrosion process. Low-carbon low-strength A516 steels are not susceptible to hydrogen embrittlement in the low temperature range at which the coupons were aged (Moody and Robinson, 1990; Gangloff, 1986; Loginow and Phelps, 1975). Tests by Loginow and Phelps on A516 pressure vessels showed that this material did not become brittle when exposed to hydrogen gas at 69 MPa (10,000 psi) for up to 5 months. In addition, examination of the failure surfaces of the "corroded" coupons under a scanning electron microscope showed ductile failure; no area(s) of brittle fracture were found.

Up to about 12% strains, the stress versus strain curve was about the same for both the corroded and uncorroded coupons. However, plate sections which had corroded were able to carry less load because the cross-sectional area had decreased. The corroded coupons failed at about 50% of the elongation that caused failure in the uncorroded specimens. This reduction was caused by very local stress and strain concentrations around pits and on the rough uneven surfaces. In these "micro" concentration regions, the plastic strains were larger than they were in areas outside of the concentration region. Failure was initiated as a result of these local plastic strains.

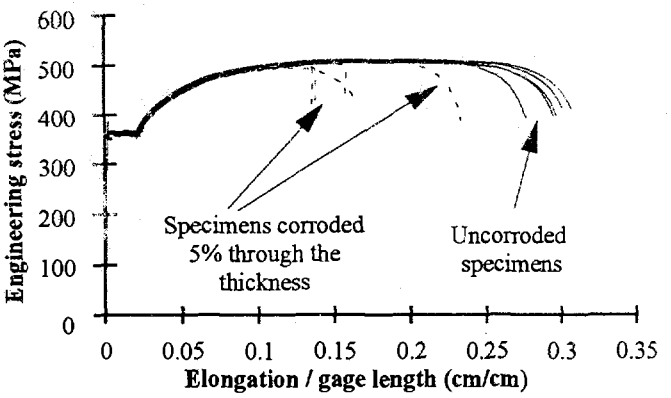

Figure 3. A516 Gr. 70 steel stress-strain curve - 5% corrosion.

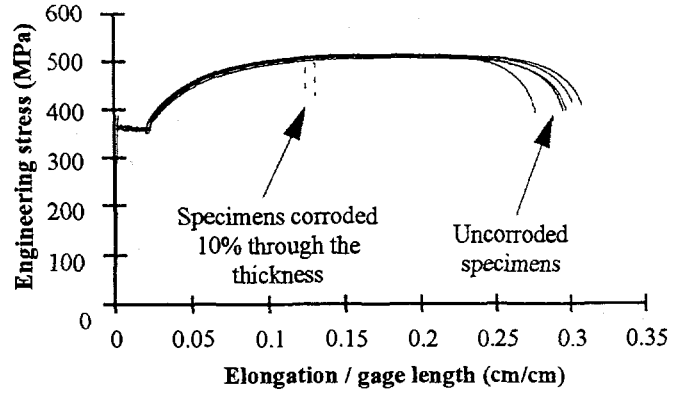

Figure 4. A516 Gr. 70 steel stress-strain curve - 10% corrosion.

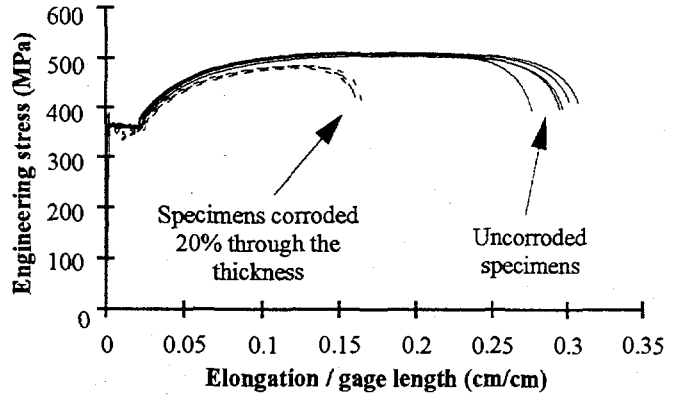

Figure 5. A516 Gr. 70 steel stress-strain curve - 20% corrosion.

ANALYSIS METHODS

Finite Element Modeling

Several scaled model containments have been tested and analyzed over the last fifteen years (Horschel, 1992, Sammataro et al., 1992, Weatherby, 1990, Clauss, 1985). The finite element analyses of these uncorroded structures showed that failure is related to local strains, and that a critical strain failure criteria can be used to predict the onset of failure. As the material strains, voids

coalesce into a flaw. At some critical strain level, the flaw reaches a critical size and a tear initiates. Most analyses that have been performed for containment structures have selected strain (or stress) based failure criteria.

Linear elastic fracture mechanics have often been used to predict critical flaw sizes in piping, in pressure vessels, and in other situations. This method has been proven and is reliable for linear, elastic problems. However, it is very difficult to apply fracture mechanics methods to highly ductile materials which undergo high strains and gross plasticity. Furthermore, it is difficult to define a traditional fracture mechanics "flaw" that represents the rough uneven surface that has been observed in corroded areas of containment vessels. Strain based criteria have been used successfully in the past, and fracture mechanics methods are difficult to apply to the corrosion damage. Therefore, a strain based failure criteria has been selected for use with finite element analyses. Sharp cracks of significant size have not been observed in corroded areas of containment structures. However, fracture mechanics methods should be considered if sharp cracks are detected during future inspections.

Strain-based failure criteria, which have been successfully used in past containment analyses, have been modified to account for corrosion effects. In the finite element model, a corroded area is modeled using the average thickness of the degraded section; the surface in the model is not rough or pitted, but is smooth. Local stress and strain concentrations that are caused by the reduced thickness and the surrounding geometry are calculated by the analysis code; the stresses and strains increase in the degraded area. The stress-strain curve used in the reduced thickness region is identical to the curve for uncorroded material, except that the critical elongation of the corroded material is decreased in accordance with the corroded coupon tests.

In the finite element model of a large structure, it is not practical to model the uneven surface of a corroded plate because of the large number of elements that would be required. Pitted and rough surfaces consist of "micro" discontinuities that are much smaller than the elements in the mesh. These "micro" discontinuities are accounted for by applying a knockdown factor to reduce the critical elongation for material in the degraded area. Stress concentrations that result from geometry changes, such as a locally thinned area or a penetration, are calculated in a finite element analysis; the concentrations that occur in "micro" areas along the pitted and rough surface are accounted for by the knockdown factor.

Failure Criteria

Failure is predicted to occur when calculated strains exceed a critical value. After a tear initiates, the failure criteria will not predict whether the tear will be unstable and propagate, resulting in catastrophic failure, or whether the crack will self-arrest and not propagate, resulting in a leak. Determining whether a crack will propagate has been tried in the past, and the results were not conclusive (Irvine and Gardner, 1983; Greimann et al., 1993). However, it appears likely that if the tear initiates in a region of high membrane strains, the tear will propagate rapidly and result in catastrophic failure. If the high strain is in a local region and the surrounding area is at a much lower strain, the failure may not be catastrophic.

Another failure criteria which is being considered, but has not been incorporated in this paper, is a displacement based criteria. Many penetrations exist in the walls of the containment structure, and excessive displacements could cause either a failure in the penetration seals, or break pipes and other items which pass through the penetrations. Many items, such as overhead cranes, are supported by the containment walls. Excessive displacement could cause these items to fall onto critical items below. However, this additional displacement failure criteria was not used in this paper.

The strain-based failure criterion that has been selected consists of applying "knockdown" factors to adjust uniaxial strain-to-failure test data. The first three factors are consistent with previous analyses (Miller, 1990, and Weatherby, 1990) and are not related to corrosion. These factors relate to the ability of the analysis model to correctly predict the structural response and to material property differences that exist in actual containments. The fourth factor has been added to account for the random effects of corrosion degradation.

Hancock et al. (1976), Mackenzie et al. (1977), Mangoine (1982), and others have shown that the critical failure strain varies as the stress state changes. The first "knockdown" factor is the Hancock and Mackenzie relationship between the triaxial stress state and the failure strain. This relationship was based on test results. The second "knockdown" factor accounts for how detailed the finite element model is. For example, the element mesh size and details missing in the model affect the accuracy of the finite element prediction. This factor approaches 1.0 as the mesh size becomes small and includes all structural details. The third "knockdown" factor accounts for the fact that in an actual structure the material properties often vary from the mean by a significant margin. For example, test data from 489 specimens used in the Sequoyah containment had yield strengths that varied from the mean by $\pm$ 12%, ultimate strengths that varied from the mean by $\pm$ 7%, and elongations that varied from the mean by $\pm$ 22%. These variations are based on a normal distribution, with 90% of the test results falling inside of the specified limits. The last "knockdown" factor accounts for corrosion degradation, and is based on the limited set of corroded coupon tests. The pitted and rough surface "micro" discontinuities are accounted for by this factor. When extrapolating corroded coupon test data to full scale containments, there is a considerable amount of uncertainty.

The critical effective plastic strain at which failure is predicted to occur is determined as:

$$\varepsilon_{failure} = \varepsilon_{uniaxial} * f_1 * f_2 * f_3 * f_4 \quad (1)$$

where

$\varepsilon_{failure}$ = effective plastic strain level at which failure is predicted to occur.

$\varepsilon_{uniaxial}$ = elongation from uniaxial tensile strain-to-failure tests.

f_1 = knockdown factor to account for multiaxial stress state,

$$= 1.648 * e^{-(\sigma_1 + \sigma_2 + \sigma_3)/2\sigma_{von}} \quad (2)$$

f_2 = knockdown factor to account for the sophistication of the analysis model.

f_3 = knockdown factor to account for variable material properties.

f_4 = knockdown factor to account for corrosion degradation.

σ_{von} = Von Mises effective stress.

$\sigma_{1,2,3}$ = principal stresses.

The f_1, f_3, and f_4 factors were estimated before analyses were performed. The f_2 factor was estimated after the analyses had completed. It was based on the amount of detail included in the finite element model in the critical failure region, and on analytical results such as strain gradients in the critical region. For each of the factors f_2, f_3, and f_4, a best estimate has been selected, along with

an upper and lower bound estimate. An upper and lower bound were not selected for the f_1 factor, which is defined by Eq. 2. These factors (Table 1) are based on engineering judgment and the data already presented. Because the stress-strain curve is fairly flat at high plastic strain levels, a large change in strain only results in a small change in the stress. Therefore, predicted failure pressures are not very sensitive to changes in the plastic strain failure criteria, and hence to the knockdown factors.

Table 1. Knockdown Factors Used in Failure Criteria.

	Factor	Lower bound	Best estimate	Upper bound
Analysis sophistication	f_2	0.40	0.50	0.60
Material properties	f_3	0.78	1.00	1.22
Corrosion	f_4	0.25	0.50	0.75

Finite element analyses that were performed are described in a later section. However, two cases required analyzing a submodel in a local region where large bending strains existed. This submodel used a fine mesh with four continuum elements through the thickness. Because of the detail, the sophistication factor (f_2) was increased to 0.9 for the lower bound, best estimate, and upper bound values for those analyses.

Minimum uniaxial strain-to-failure values for elongation in a 20.3 cm (8 in.) gage length are given in the ASME code as 21% for A516 Grade 60 steel. For actual specimens, the elongation at failure is well above the 21% minimum; however, the load carrying capacity of the specimens began to decrease significantly around 21%, with total failure occurring at higher levels. Using $\varepsilon_{uniaxial} = 21\%$, and the knockdown factors from Table 1, the failure curves for A516 Grade 60 steel were calculated (Fig. 6) using Eqs. 1 and 2. Since only a small portion of the total surface of a containment was corroded in the analyses, the failure strains are given for both the corroded and uncorroded states. In the analyses, the uncorroded failure strains were used to predict failure of the portions of the containment that were not corroded, and the corroded failure strains were used to predict failure of the corroded sections.

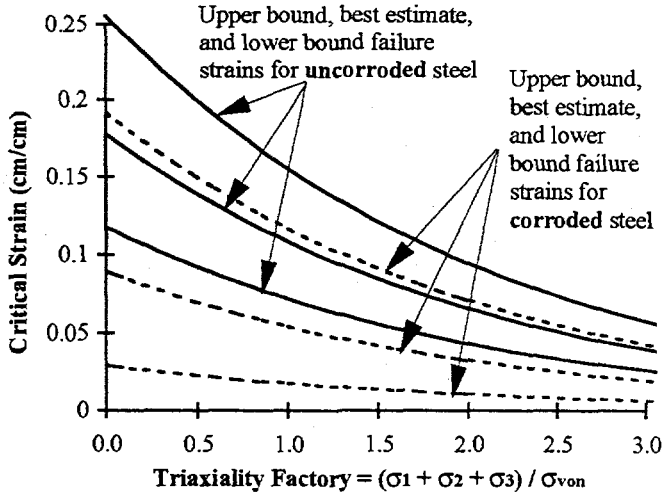

Figure 6. Failure Curves for A516 Grade 60 Steel.

ANALYSES OF A "TYPICAL" PWR ICE CONDENSER CONTAINMENT

A U.S. Nuclear Regulatory Commission report (Shah et al., 1994) gives a thorough listing of nuclear power plant containment structures, typical design parameters, the materials used in the structures, environmental operating conditions, types of corrosion that can be expected for the materials involved, and the locations on the containment structures where the corrosion is likely to occur. They also provide detailed descriptions of corrosion degradation that has been observed in containments of operational nuclear power plants.

Geometry

The typical PWR Ice Condenser containment (Fig. 7) is a circular cylinder capped with a hemispherical dome, and is constructed entirely from A516 Grade 60 steel. The cylindrical section has a diameter of 35 m, and the height from its base to the top of the dome is about 53 m. The shell thickness varies from 3.49 cm at the bottom, to 1.11 cm at the top of the cylinder, and then increases back to 2.38 cm at the top of the dome. The shell is 3.81 cm thick in the vicinity of pipe penetrations, airlocks, and other openings. Welded to the exterior of the shell is a web of vertical stringers, horizontal stiffeners, and other miscellaneous structures. The vertical stringers are spaced every four degrees circumferentially, and the horizontal stiffeners are about 2.9 m apart. The shell is embedded in and anchored to a reinforced concrete basemat.

Three areas that were degraded in the finite element model were: the region around the ice basket, a ring area near the basemat, and a ring area at the upper floor level. In actual containments, the region around the ice basket has a high potential for corrosion, but the status is unknown because the area is inaccessible for inspections. During inspections, corrosion damage has been observed near the basemat and at the upper and lower floor levels (Figs. 8 and 9).

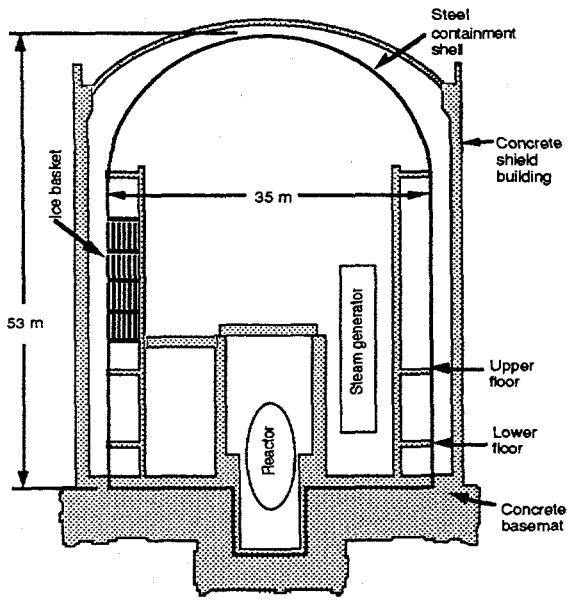

Figure 7. "Typical" PWR Ice Condenser containment.

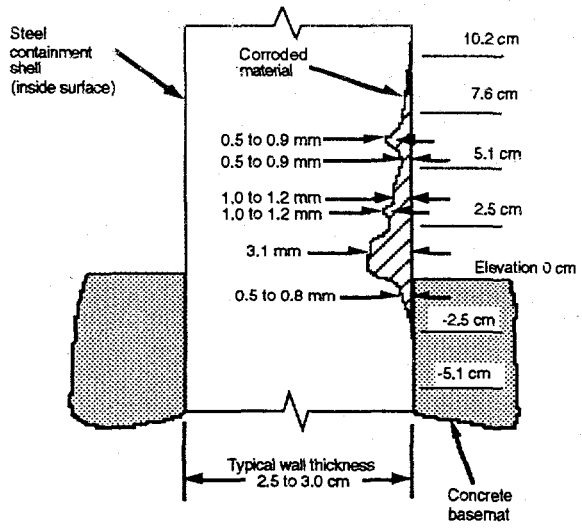

Figure 8. Observed damage to steel shell near basemat.

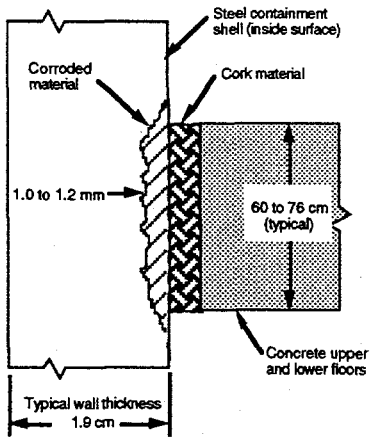

Figure 9. Observed damage near upper and lower floor.

Finite Element Model

The ABAQUS finite element model (Fig. 10) consisted of 10125 four-node quadrilateral shell elements (S4R) and 10325 nodes. It included a 53° circumferential segment of the containment, and went from the concrete basemat to the top of the dome. This segment, which had symmetry boundary conditions applied to it, was representative of a typical containment. Vertical stringers and the horizontal stiffeners were included in the model. The smallest elements had a side length of about 10 cm, while the average element had a length of about 30 cm (1° circumferentially). The concrete basemat was not modeled since it had been studied previously (Fanous et al., 1993). The penetrations were not explicitly modeled either. In previous analyses (Miller, 1990; Greimann, et al., 1984) it was found that containment failure occurred where thin wall sections met the thicker plate sections that the penetrations passed through (Clauss, 1985; Greimann et al., 1987). In these studies, plastic yielding occurred in the thinner plate sections, and not in the thickened plates. Bellows were addressed under a previous program (Lambert, et al., 1995).

The containment was modeled to determine failure level and location under several different degraded conditions. Three areas on the containment surface that were degraded (Fig. 10) correspond to the damaged or susceptible areas identified at nuclear power plants. In these areas corrosion was modeled by thinning shell elements and reducing the critical plastic failure strains (Fig. 5). The depth of the corrosion was selected to ensure that failure occurred in the degraded area. Greater than 50% through the thickness damage was required at two locations to cause a failure in the degraded area. The containment was analyzed in seven different configurations, with:

- No corrosion present.
- Corrosion near the top of the ice basket, with a 10% through the thickness corroded area of 1.09 m high by 0.91 m circumferentially. In operational containments, this area is susceptible to corrosion, but is inaccessible and does not get inspected. Analyses show this is the area of highest strains on an uncorroded containment, and the expected failure location.
- Corrosion near the top of the ice basket, as described above, except the damage is 25% through the thickness.
- Corrosion in the steel shell at the upper floor level, with a 50% through the thickness corroded area of 0.81 m high by 11.94 m around the circumference. Corrosion has been found in this location during inspections at the Catawba and McGuire plants.
- Corrosion at the upper floor level, as described above, except the damage is 65% through the thickness.
- Corrosion in the steel shell near the concrete basemat, with a 50% through the thickness corroded area of 0.102 m high by 3.99 m around the circumference. Corrosion has been observed here during inspections at the Catawba and McGuire plants.
- Corrosion in the concrete basemat region, as described above, except the damage is 65% through the thickness.

Material Properties

Previous finite element analyses have been performed for the Sequoyah containment building (Miller, 1990). To support that and similar efforts, work-hardening data was obtained by testing A516 Grade 70 steel at 22, 93, 149, and 204°C (Fatigue Technology Inc., 1988). A516 Grade 60 temperature-dependent material properties were estimated (Fig. 11) by adjusting for the difference in yield strength between Grade 70 and Grade 60 steel. The coefficient of thermal expansion of the steel was determined to be 11.3 X 10^{-6}/°C over the range from 22 to 204°C.

Loads

Each model was loaded with quasi-static internal pressure that increased monotonically. During many postulated accidents, the pressure is caused by water turning into steam. Therefore, a thermal load was simultaneously applied to all steel parts above the concrete basemat; the temperature of the containment shell followed a saturated steam pressure vs. temperature relationship (Fig. 12). An initial stress-free state was assumed to exist at 22°C. As the pressure was increased, the temperature at every node in the model that was above the concrete basemat was increased to correspond to the saturated steam relationship.

Analysis Results

Analyses were performed using the ABAQUS finite element code. Elements in the model did not automatically fail when they

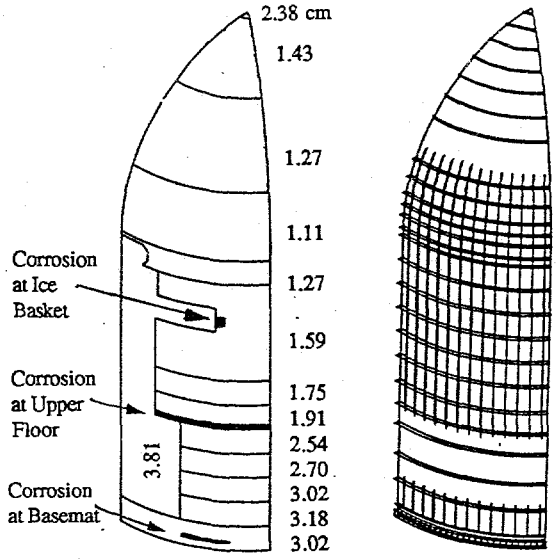

Figure 10. Finite element model shell thicknesses and stringer and stiffener locations.

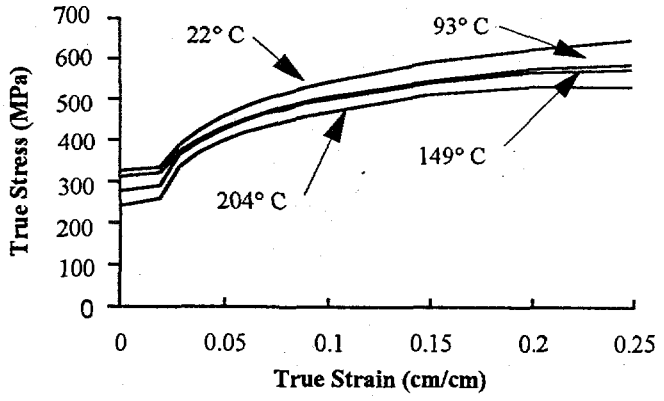

Figure 11. A516 Grade 60 temperature dependence.

reached the critical strain values. Instead, failure predictions were assessed during post-processing. Failure was predicted when any element in the model reached the critical strain level.

In each of the analyses, failure was predicted to occur in a cylindrical section, and in each case the triaxiality factor (Fig. 6) was very close to 1.73. As the loads were increased and the material plastically strained, the triaxiality factor varied only a small amount. This was because each of the critical failure locations was in a cylindrical section. If a point on the spherical dome had been selected, the triaxiality factor would have been close to 2. An element in uniaxial tension, such as a bolt, would have had a triaxiality factor of 1. However, at the three locations where failure was predicted to occur, the triaxiality factor was 1.73.

For each analysis, failure predictions consisted of a "lower bound" failure pressure, a "best estimate" failure pressure, and an "upper bound" failure pressure. With a triaxiality factor of 1.73 and the failure model shown in Fig. 6, the lower bound, best estimate, and upper bound critical membrane strains for uncorroded material were 4.5, 7.3, and 10.6%, respectively. For material that was corroded, the lower bound, best estimate, and upper bound critical membrane strains were 1.1, 3.6, and 8.0%, respectively. The critical values allowed for bending strains were increased by 50%.

The effective plastic strains for the uncorroded containment (Figs. 13 and 14) showed a few areas that experienced large plastic membrane strains. For the uncorroded containment, failure would be expected to occur at the high strain location around the ice basket. At this location a 3.81 cm thick plate protruded into a 1.59 cm thick area and caused large membrane strains in the thinner plate. A few other locations on the model with a thick section protruding into a thinner area also showed a region of large membrane strains in the thinner plate near the discontinuity. These strains were considerably larger than free field strains in the thin plate. However, many areas where thick plates transitioned to thin plates did not experience larger-than-free-field strains in the region near the weld joint. From Fig. 13 it can be seen that large plastic strains were only reached in a few regions, and that the global, free-field strains were considerably lower.

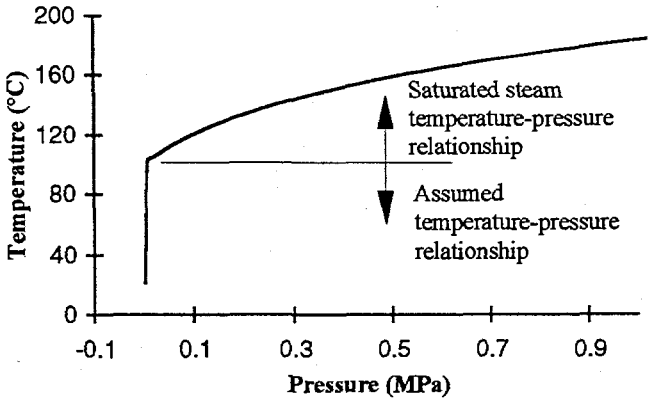

Figure 12. Saturated steam temperature-pressure relationship.

The analyses that included "corrosion" had higher strains in the locally thinned areas than corresponding strains in the undegraded case. Although the strains were higher in the locally thinned areas, the global responses were very similar to the response of a containment with no corrosion damage.

Because of significant bending near the basemat, a finely meshed submodel of the area was analyzed. Since the finite element mesh was much finer, the "sophistication" knockdown factor (f_2) was increased to 0.9 for the lower bound, best estimate, and upper bound cases. This resulted in critical values for bending strains in the submodel of 3.8, 9.8, and 18% for the lower, mid, and upper bound criteria. Predicted failure results (Table 2) show that corrosion in the area of highest strain will significantly reduce the pressure capacity of the vessel, while considerable corrosion in other areas can be tolerated without reducing the pressure capacity. The design pressure for the containment modeled was 0.074 MPa (10.8 psi).

The structural response of the first five cases (Table 2) was primarily membrane. Membrane forces in the cylindrical portion of the structure were twice as large in the circumferential direction as they were in the vertical direction. This is a known behavior of cylindrical sections. In the first three cases, internal pressure caused the structure to radially expand until failure occurred in the

Table 2. Predicted Failure Pressures

Case No.	Description	Failure Pressure		
		Lower bound	Best estimate	Upper bound
1	no corrosion	0.43 MPa (63 psi)	0.47 MPa (68 psi)	0.54 MPa (78 psi)
2	10% corrosion at ice basket	0.40 (58)	0.43 (63)	0.48 (69)
3	25% corrosion at ice basket	0.39 (56)	0.43 (62)	0.45 (65)
4	50% corrosion at upper floor	0.43 (62)	0.47 (68)	*
5	65% corrosion at upper floor	0.35 (51)	0.44 (64)	0.47 (68)
6	50% corrosion at basemat	0.30 (43)	*	*
7	65% corrosion at basemat	0.28 (41)	0.47 (68)	*

* Failure is not predicted to occur at the corroded location.

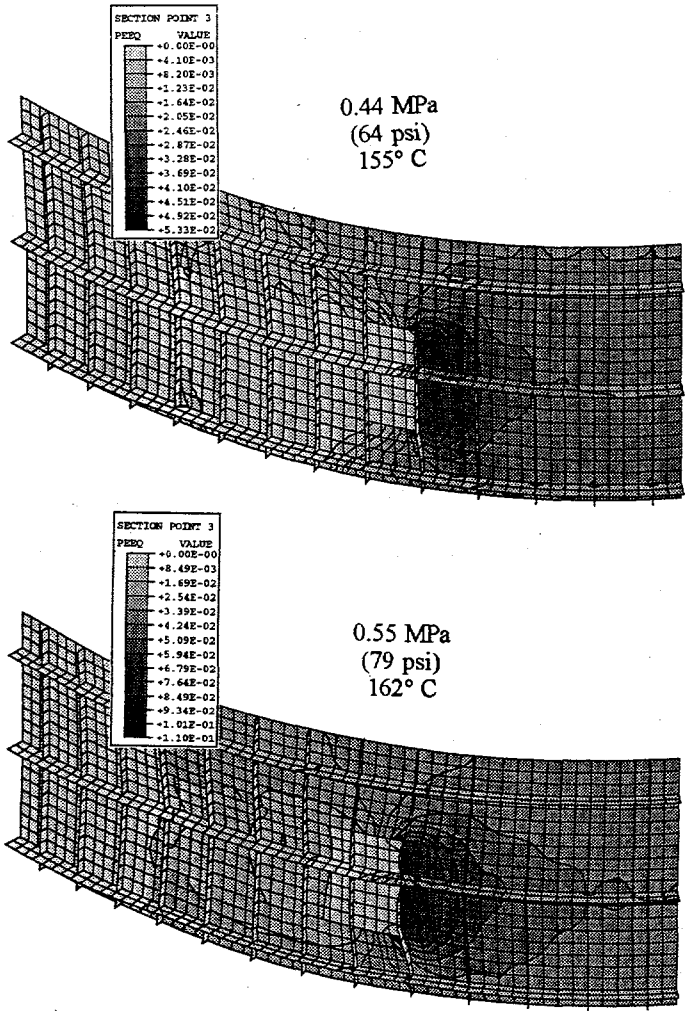

Figure 13. Plastic membrane strain (uncorroded containment) at highest strain region by Ice Basket.

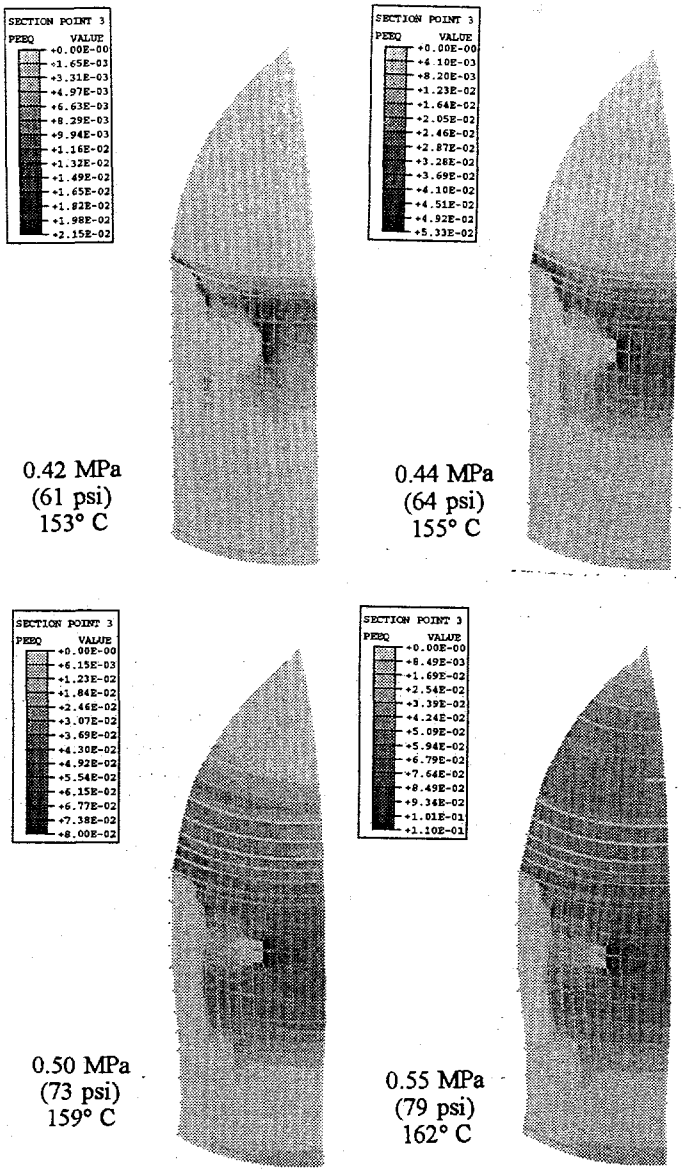

Figure 14. Plastic membrane strain (uncorroded containment) with displacements magnified by a factor of 5.

circumferential direction. Even while the structure was plastically flowing in the hoop direction, there was minimal plastic growth in the vertical direction. For these three cases, failure was predicted to occur near the top of the ice basket as a result of large hoop strains. In cases 2 and 3, the corrosion was located in the area of highest plastic strain. As expected, even small amounts of corrosion in high strain regions caused failure to occur at lower pressures. In cases 4 and 5, the thinned section was only 0.81 m high, but extended 11.9 m in the circumferential direction. The thicker sections above and below this degraded area were stiff enough that they did not undergo large hoop strains, and this support prevented the thinned section from experiencing large plastic hoop strains. It was not until the thickness of the corroded section was decreased by a factor of two that the vertical component of stress

became large enough to cause large plastic membrane strains in the vertical direction, and failure was predicted at this location. For cases 6 and 7, the steel shell was relatively thick near the basemat and was embedded in the concrete floor. Circumferential straining in the thinned section at the basemat was limited because of support from the basemat and the thick plate above the reduced area. It was not until the thickness of the corroded section was decreased by a factor of two that the vertical component of stress became large enough to cause large plastic strains in the vertical direction. In this case, however, the peak strains were a result of membrane and bending in the vertical direction.

CONCLUSIONS

The corrosion damage in existing containments has often been in a horizontal plane, such as along the upper and lower floors and at the basemat level (Figs. 8 and 9). For a cylindrical structure, a narrow band of thinned material that extends around the circumference can often be tolerated because the surrounding structure is often stiff enough to prevent the degraded area from large plastic hoop strains. However, if a narrow band of corrosion occurred in the vertical direction on a cylindrical containment, the reduction in capacity would be more severe. This is because internal pressure causes a larger membrane force in the hoop direction than in the vertical direction. In the corrosion that was modeled around the ice basket, failure occurred through large plastic strains that grew circumferentially. The geometry of the structure caused large membrane hoop strains in the thinned area, and the structure expanded in the radial direction. Therefore, any amount of corrosion near the ice basket high strain region degraded the load-carrying capacity.

ACKNOWLEDGMENTS

James Costello and Wallace Norris, from the U.S. Nuclear Regulatory Commission, have been instrumental in developing this program.

REFERENCES

ASME Boiler & Pressure Vessel Code, 1992, Section III, Division 1, Appendix I, Figure I-9.1.

ASTM, 1991, "Standard Test Methods of Tension Testing of metallic Materials," Designation E8 - 91.

Clauss, D. B., 1985, "Comparison of Analytical Predictions and Experimental Results for a 1:8-Scale Steel Containment Model Pressurized to Failure," NUREG/CR-4209, SAND85-0679, Sandia National Laboratories, Albuquerque, NM.

Fanous, F., Greimann, L., Wassef, W., and Bluhm, D., 1993, "Performance of Sequoyah Containment Anchorage System," SAND92-7308, IS-5012, Ames Laboratory, Iowa State University, IA.

Fatigue Technology Inc., 1988, "Sandia High Temperature Tensile Test Report," FTI Test Report 8057-1, Fatigue Technology Inc., Seattle, Washington.

Gangloff, R. P., 1986, "A Review and Analysis of the Threshold for Hydrogen Environment Embrittlement of Steel," Corrosion Prevention and Control, Proc. 33rd Sagamore Army Materials Research Conference, S. Isserow, ed.

Greimann, L., Fanous, F., Rogers, J., and Bluhm, D., 1987, "An Evaluation of the Effects of Design Details on the Capacity of LWR Steel Containment Buildings," NUREG/CR-4870, SAND87-7066.

Greimann, L., Fanous, F., and Bluhm, D., 1984, "Final Report, Containment Analysis Techniques, A State-of-the-Art Summary," NUREG/CR-3653, Ames Laboratory, IA.

Hancock, J. W., and Mackenzie, A. C., 1976, "On the Mechanisms of Ductile Failure in High-Strength Steels Subjected to Multi-Axial Stress States," *Journal of Mechanics and Physics of Solids*, Vol. 24, pp. 147-169.

Horschel, D. S., 1992, "The Design, Fabrication, Testing, and Analyses of Four 1:32-Scale Steel Containment Models," SAND84-2153, Sandia National Laboratories, Albuquerque, NM.

Irvine, W. H., and Gardner, C. J., 1983, "Pneumatic Burst Test Under 'Upper Shelf Conditions' of a Pressure Vessel Containing an Axial Defect," United Kingdom Atomic Energy Authority, Safety and Reliability Directorate, Warrington.

Jung, J., 1984, "Ultimate Strength Analyses of the Watts Bar, Maine Yankee, and Bellefonte Containments," NUREG/CR-3724, SAND84-0660, Sandia National Laboratories, Albuquerque, NM.

Koenig, L. N., 1986, "Experimental Results for a 1:8-Scale Steel Model Nuclear Power Plant Containment Pressurized to Failure," NUREG/CR-4216, SAND85-0790, Sandia National Laboratories, Albuquerque, NM.

Lambert, L. D., and Parks, M. B., 1995, "Experimental Results From Containment Piping Bellows Subjected to Severe Accident Conditions," Vol. 1 and 2, NUREG/CR-6154, SAND94-1711, Sandia National Laboratories, Albuquerque, NM.

Loginow, A. W., and Phelps, E. H., 1975, "Steels for Seamless Hydrogen Pressure Vessels," *Corrosion*, Vol. 31, No. 11, pp. 404-412.

Mackenzie, A. C., Hancock, J. W., and Brown, D. K., 1977, "On the Influence of State of Stress on Ductile Failure Initiation in High Strength Steels," *Engineering Fracture Mechanics*, Vol. 9, pp. 167-188.

Mangoine, M. J., 1982, "Creep-Rupture Behavior of Weldments," *Welding Journal Research Supplement*, Vol. 61, No. 2, American Welding Society.

Miller, J. D., 1990, "Analysis of Shell-Rupture Failure Due to Hypothetical Elevated-Temperature Pressurization of the Sequoyah Unit 1 Steel Containment Building," NUREG/CR-5405, SAND89-1650, Sandia National Laboratories, Albuquerque, NM.

Moody, N. R., Robinson, S. L., and Garrison, W. M. Jr., 1990, "Hydrogen Effects on the Properties and Fracture Modes of Iron-Based Alloys," *Res Mechanica*, Vol. 30, pp. 143-206.

Reese, R. T., and Horschel, D. S., 1985, "Design and Fabrication of a 1/8-Scale Steel Containment Model," NUREG/CR-3647, SAND84-0048, Sandia National Laboratories, Albuquerque, NM.

Sammataro, R. F., Solonick, W. R., and Edwards, N. W., 1992, "A Generic Approach for Containment Success Criteria Under Severe Accident Loads," Proceedings of the Fifth Workshop on Containment Integrity, NUREG/CP-0120.

Shah, V. N., Sinha, U. P., and Smith, S. K., 1994, "Insights for Aging Management of Light Water Reactor Components, Metal Containments," NUREG/CR-5314, EGG-2562, Vol. 5, Idaho National Engineering Laboratory, Pocatello, ID.

Shigley, J. E., 1983, *Mechanical Engineering Design*, 2nd edition, McGraw-Hill, New York.

Structural Alloys Handbook, 1989, Vol. 3, Metals and Ceramics Information Center, Battelle, Columbus, OH.

Weatherby, J. R., 1990, "Posttest Analysis of a 1:6-Scale Reinforced Concrete Reactor Containment Building," NUREG/CR-5476, SAND89-2603, Sandia National Laboratories, Albuquerque, NM.